Doppler Correction of Wave Frequency Spectra Measured by Underway Vessels

C. O. COLLINS III,[a] B. BLOMQUIST,[b] O. PERSSON,[b] B. LUND,[c] W. E. ROGERS,[a] J. THOMSON,[d] D. WANG,[a] M. SMITH,[d] M. DOBLE,[e] P. WADHAMS,[f] A. KOHOUT,[g] C. FAIRALL,[b] AND H. C. GRABER[c]

[a] *Oceanography Division, U.S. Naval Research Laboratory, Stennis Space Center, Mississippi*
[b] *National Oceanic and Atmospheric Association/Earth System Research Laboratory, Boulder, Colorado*
[c] *Department of Ocean Sciences, Rosenstiel School of Marine and Atmospheric Science, University of Miami, Miami, Florida*
[d] *Applied Physics Laboratory, University of Washington, Seattle, Washington*
[e] *Polar Scientific Ltd., Appin, Argyll, Scotland*
[f] *Department of Applied Mathematics and Theoretical Physics, Cambridge University, Cambridge, United Kingdom*
[g] *National Institute of Water and Atmospheric Research, Auckland, New Zealand*

ABSTRACT

''Sea State and Boundary Layer Physics of the Emerging Arctic Ocean'' is an ongoing Departmental Research Initiative sponsored by the Office of Naval Research (http://www.apl.washington.edu/project/project.php?id=arctic_sea_state). The field component took place in the fall of 2015 within the Beaufort and Chukchi Seas and involved the deployment of a number of wave instruments, including a downward-looking Riegl laser rangefinder mounted on the foremast of the R/V *Sikuliaq*. Although time series measurements on a stationary vessel are thought to be accurate, an underway vessel introduces a Doppler shift to the observed wave spectrum. This Doppler shift is a function of the wavenumber vector and the velocity vector of the vessel. Of all the possible relative angles between wave direction and vessel heading, there are two main scenarios: 1) vessel steaming into waves and 2) vessel steaming with waves. Previous studies have considered only a subset of cases, and all were in scenario 1. This was likely to avoid ambiguities, which arise when the vessel is steaming with waves. This study addresses the ambiguities and analyzes arbitrary cases. In addition, a practical method is provided that is useful in situations when the vessel is changing speed or heading. These methods improved the laser rangefinder estimates of spectral shapes and peak parameters when compared to nearby buoys and a spectral wave model.

1. Introduction

The problem of calculating 1D and 2D wave spectra from a time series recorded on a moving vessel has been discussed in previous studies (Drennan et al. 1994; Hanson et al. 1997; Cifuentes-Lorenzen et al. 2013). The theory used in these studies can be traced back to the work of Kats and Spevak (1980). Although the theory is general and considers both scenarios of steaming into waves (referred to as ''into-waves'') and steaming with waves (''with-waves''), previous field studies analyzed only a small subset of cases in the into-waves scenario. This was likely to avoid the ambiguities that arise steaming with-waves. This study goes a step further by making a practical assumption to handle the ambiguities, which opens up the analysis of arbitrary cases.

a. The intrinsic frequency spectrum

In the absence of currents, the linear dispersion relationship for deep-water waves relates the intrinsic frequency f_{in} to the wavenumber k (e.g., Lamb 1932; Kinsman 1965):

$$f_{in} = \sqrt{gk}/2\pi, \tag{1}$$

where g is acceleration due to gravity. Under the influence of a current, the wave signal observed in an Eulerian reference frame is Doppler shifted according
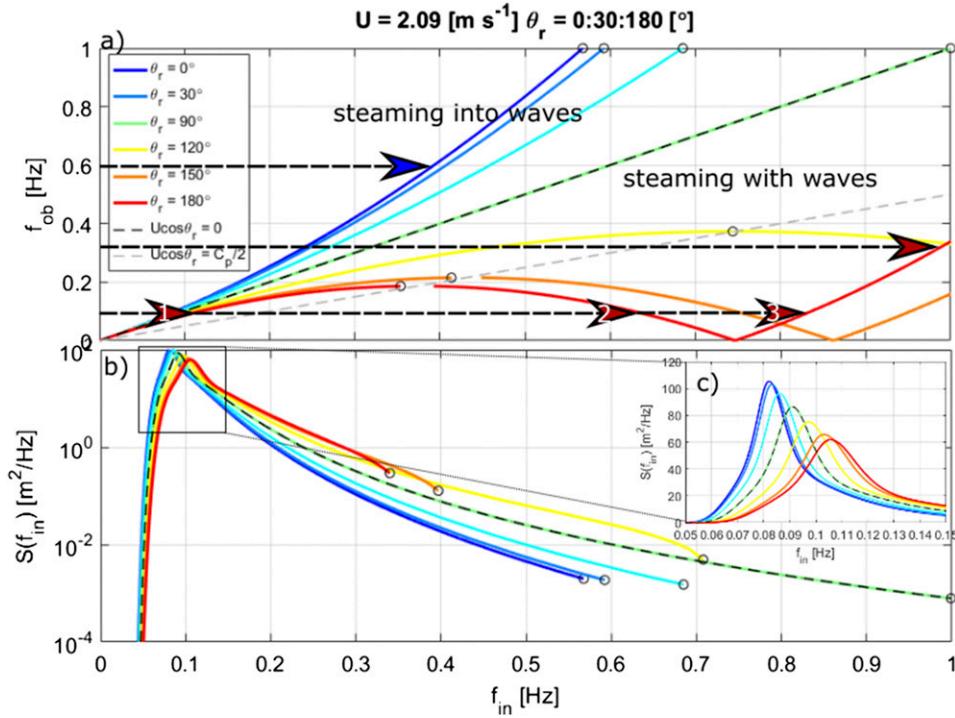
FIG. 1. (a) Mapping between intrinsic frequencies and observed frequencies for $U = 2.09 \, \text{ms}^{-1}$. Colors indicate the value of θ_r from 0° (blue) to 180° (red). Dashed gray line is the critical frequency [Eq. (10)]. Black circles give the last frequency bin. Black dotted line is a reference for the case of $\theta_r = 90°$ that divides (a) in half diagonally. Bottom-right side of the black diagonal shows mapping for the case of steaming with waves (warm colors) and the top-left side for steaming into waves (cool colors). Arrows in (a) point from the observed frequency to intrinsic frequencies: from 0.6 Hz with $\theta_r = 0°$ (blue) to 0.3 Hz with $\theta_r = 180°$ (red). From 0.1 Hz, the arrows with numbers show the three different contributions of intrinsic frequencies to observed frequency. (b) Demonstration of the resulting wave spectra from the corresponding Doppler correction. Solid black line is an unadjusted JONSWAP spectrum. Black circles indicate the last spectral component, one frequency bin lower than the corresponding black circles in (a). (c) Zoom-in view of the spectral peak.

to the relative angle between the mean current and the wave direction (θ_w). Analogously, a sensor mounted on an underway vessel—for example, ships, submarines, unmanned or autonomous underwater vehicles, even airborne sensors and drones—introduces a Doppler component that relates the observed frequency f_{ob} to f_{in}:

$$f_{ob} = \frac{1}{2\pi}[\sqrt{gk} + \mathbf{k} \cdot \mathbf{U}] = f_{in} + \frac{|\mathbf{k}||\mathbf{U}|\cos\theta_r}{2\pi}. \quad (2)$$

Here $\mathbf{U}$ is the velocity vector of the vessel, $\mathbf{k}$ is the wavenumber vector, and θ_r is the relative angle between the vessel heading θ_s and wave direction θ_w (using "coming-from" convention). Solving for f_{in} and dropping the magnitude notation results in

$$f_{in} = f_{ob} - \frac{kU\cos\theta_r}{2\pi}, \quad (3)$$

where k is invariant between reference frames and can be written in terms of the f_{ob} (Drennan et al. 1994):

$$k = \frac{g + 4\pi f_{ob}U\cos\theta_r - \sqrt{g^2 + 8\pi g f_{ob}U\cos\theta_r}}{2U^2\cos^2\theta_r}. \quad (4)$$

In terms of f_{ob}, f_{in} is

$$f_{in} = f_{ob} - \frac{g + 4\pi f_{ob}U\cos\theta_r - \sqrt{g^2 + 8\pi g f_{ob}U\cos\theta_r}}{4\pi U\cos\theta_r}. \quad (5)$$

This is one solution to mapping frequencies from f_{ob} to f_{in}; a second root is also possible (not shown) that becomes relevant in the discussion of Fig. 1 in section 1b. Doppler correction (DC) changes the frequency resolution, so a Jacobian is required to conserve spectral energy S:

$$S_{\text{in}}(f_{\text{in}}) = S_{\text{ob}}(f_{\text{ob}}) \frac{\delta f_{\text{ob}}}{\delta f_{\text{in}}}, \qquad (6)$$

where δ indicates the bin width, determined here by simple finite differencing.

b. Frequency mapping scenarios

Assuming a constant vessel heading and speed over the analysis window and zero current, the remaining unknown is θ_w, which in practice must be measured or assumed. In a typical field experiment, potential sources of θ_w may be drift direction, wind direction, wave model, buoy measurement, or marine radar (MR) measurement. Given a source for θ_w, f_{ob} can be mapped to f_{in}.

An illustration of this mapping is represented in Fig. 1a, where varying θ_r is represented by colored lines in 30° increments for a vessel speed of 2.09 m s^{-1}. A half-plane of directional space is represented, with the center direction, 90°, being a vessel heading orthogonal to the θ_w.

Steaming into-waves is represented by the range of $\theta_r = 0°$–90° (cool colors): f_{ob} always maps to a lower value of f_{in} and there is no ambiguity. For the case of $\theta_r = 0°$, a f_{ob} of 0.6 Hz results in a f_{in} of 0.37 Hz.

Steaming with waves is represented by the range of $\theta_r = 90°$–180° (warm colors): For $\theta_r = 180°$ f_{ob} increases with f_{in} from $f_{\text{in}} = 0$–0.34 Hz, then f_{ob} bends back to lower frequencies until it reaches 0 at $f_{\text{in}} = 0.75$ Hz, and then f_{ob} again returns to higher frequencies. For a range of f_{ob}, there are contributions from two or more f_{in}. It is impossible to determine the allocation of energy attributable to each f_{in}; the solution is intrinsically ambiguous.

Consider the case of $\theta_r = 180°$ (red line in Fig. 1a) and a spectrum of waves on the sea surface. A ship propagates in the direction of the waves, and each wave crest propagates with a phase speed $C_p(f_{\text{in}})$ that is highest for low-frequency waves and decreases as the frequency increases. Following the red line and starting in the low f_{in}—as f_{in} increases the corresponding f_{ob} increases—these waves are propagating faster than twice the vessel speed. As f_{in} further increases the corresponding f_{ob} decreases, and the phase speed in this band is less than twice the ship speed but still greater than the ship speed. As the phase speed of f_{in} approaches the vessel speed, f_{ob} approaches zero. With increasing f_{in}, the phase speed is slower than the vessel speed and the waves are being overtaken by the vessel. In this band, the f_{ob} continues to decrease as f_{in} increases. The f_{ob} is now negative and further decreases as f_{in} increases (shown in Fig. 1 by plotting on the positive y axis).

The arrows show that contributions to the energy at $f_{\text{ob}} = 0.10$ Hz originate, in order of increasing f_{in}, from

arrow 1 $\sim$ 0.11, arrow 2 $\sim$ 0.61, and arrow 3 $\sim$ 0.84 Hz. The first contribution comes from long, fast waves:

$$C_p(f_{\text{in}}) > 2U \cos\theta_r. \qquad (7)$$

For f_{in} with phase speeds more than twice the vessel speed, the branch of the solution (arrow 1) is given by Eq. (5). Arrow 2 points to a contribution from the f_{in} of a wave with intermediate speed $2U \cos\theta_r > C_p(f_{\text{in}}) > U \cos\theta_r$ and is given by the other root (the same equation with one sign change):

$$f_{\text{in}} = f_{\text{ob}} - \frac{g + 4\pi f_{\text{ob}} U \cos\theta_r + \sqrt{g^2 + 8\pi g f_{\text{ob}} U \cos\theta_r}}{4\pi U \cos\theta_r}. \qquad (8)$$

Arrow 3 is the contribution from the vessel overtaking waves, $C_p(f_{\text{in}}) < U \cos\theta_r$, and is given by Eq. (8) above but using negative f_{ob}:

$$f_{\text{in}} = -f_{\text{ob}} - \frac{g - 4\pi f_{\text{ob}} U \cos\theta_r + \sqrt{g^2 - 8\pi g f_{\text{ob}} U \cos\theta_r}}{4\pi U \cos\theta_r}. \qquad (9)$$

As f_{ob} increases, the ambiguity reduces when the phase speed is twice the vessel speed:

$$C_p = 2U \cos\theta_r. \qquad (10)$$

Here there are only two contributing frequencies because the solutions for lower frequencies converge, and this frequency is referred to as the critical frequency f_{cr}.

There is no ambiguity for f_{ob} higher than the corresponding f_{cr}. For example, for $\theta_r = 180°$ the arrow from f_{ob} of 0.30 Hz comes only from f_{in} of 0.98 Hz. To resolve the ambiguities at $f < f_{\text{cr}}$, all the spectral energy is attributed to intrinsic frequencies of the lowest frequency branch. This choice results in an information gap in f_{in} because of a discontinuity in the mapping. For $\theta_r = 180°$ at f_{cr}, f_{ob} is 0.20 Hz and is mapped to f_{in} of 0.37 Hz; the next lower f_{ob} bin will be mapped to f_{in} of $\sim$0.9 Hz, leaving a $\sim$0.5-Hz gap. In practice, an unambiguous spectral range up to 0.37 Hz may be adequate, but as the vessel speed increases f_{cr} decreases, further reducing the spectral range.

A demonstration of the effect of changing θ_r on calculating the S_{in} from an observed wave spectrum is shown in Fig. 1b. The dashed black curve shows a JONSWAP spectrum for $\theta_r = 90°$ (unaffected by DC) defined up to 1.0 Hz. Figure 1c shows a close-up of the spectral peak. For $\theta_r = 0°$, the peak frequency f_p shifts from 0.090 to 0.081 Hz and for $\theta_r = 180°$ to 0.105 Hz. The black circles in the with-waves section of Fig. 1a are the last frequency

bin below f_{cr}. Because the frequency difference between neighboring frequency bins is required to evaluate the Jacobian, the high-frequency cutoff of the spectrum is in practice two frequency bins below f_{cr} (black circles in Fig. 1b), rather than the last frequency bin below f_{cr} as for Fig. 1a. Steaming into-waves also results in a reduced spectral range that depends on the mapping of the last observed frequency at the Nyquist limit (see discussion in Cifuentes-Lorenzen et al. 2013).

2. Methods

a. Arctic Sea State Experiment

During the 2015 Office of Naval Research–sponsored ''Sea State and Boundary Layer Physics of the Emerging Arctic Ocean''[1] (Thomson et al. 2013), a downward-looking laser rangefinder was mounted on the R/V *Sikuliaq* foremast about 15 m above the mean water level. Sea surface elevation data were recorded at 10 Hz in the ship reference frame. This was converted to an Earth reference frame (with respect to the mean sea level) with a collocated inertial motion unit (IMU) that recorded ship motion. For the purpose of DC, the ship speed and heading were determined from the ship's GPS record, sampled every minute. A marine X-band radar (MR) provided underway directional wave and current results (Lund et al. 2015, 2016). Further details can be found in the supplemental material.

The analysis was focused on a 3-day storm period from 11 to 13 October 2015 called wave array 3 (WA3). During WA3 a number of wave sensors were deployed in a linear array, including University of Washington Surface Wave Instrument Float with Tracking (SWIFT) buoys (Thomson 2012), Cambridge University buoys, and a buoy developed at New Zealand's National Institute of Water and Atmospheric Research (similar to Kohout et al. 2015). The sea state around the peak of the storm was a wind sea with a significant wave height of 4–5 m, an f_p of ~0.10 Hz, and an east-southeast direction.

b. Quality control and ship motion diagnostics

The window chosen for calculating spectra from a time series must be a balance between reducing the statistical uncertainty (by using a longer window) and satisfying the assumption of stationarity of the ever-changing sea state (by using a shorter window). Typically, 10–60 min is acceptable. A vessel's heading and speed needed be constant for the analysis period for the most accurate DC. However, this ideal is rarely realized in practice, as the

heading and speed are subject to competing mission requirements. The changing speed and direction introduce errors into the DC; this fact motivated the design of two methods. Both methods begin with time series of ship speed and heading sampled every minute and sea surface elevation sampled at 10 Hz and end with a spectra representative of a 1-h window.

Simple method (SM): Calculate S_{ob} from hourly time series of sea surface elevation. Calculate S_{in} using ship speed and heading averaged over the hour. Use the standard deviation of ship speed and heading as a quality control flag.

Ensemble method (EM): Split hourly time series into ten 6-min sections. For each section, calculate 10 S_{ob} and then 10 S_{in}. A member section is discarded if the standard deviation of speed was $\sigma(U) > 0.5\,\mathrm{m\,s}^{-1}$ or if the directional equivalent of standard deviation of heading was $\sigma_\theta(\theta_s) > 15°$, then the remaining S_{in} were averaged together for a 1-h ensemble. Individualizing the DC for each section results in a more accurate correction for each member; however, as more member spectra are discarded, the statistical uncertainty of the ensemble spectrum increases by reducing the statistical degrees of freedom.

Two sources of θ_w were tested. The first used an ostensible θ_w, parallel to the sensor array and constant in time: 335°. The second source was the peak of the MR directional wave spectrum produced by the marine radar (see supplemental document).

The ice concentration (not shown) increased along the array from the southeast to the northwest. The ice was predominantly pancakes with a typical diameter of 5–10 cm in a frazil matrix (comparable to the case of Doble et al. 2015), the presence of which damps the high-frequency tail of the wave spectrum (e.g., Wadhams et al. 1988).

3. Results

For spectral plots and quantitative statistics, all available buoys were used; the spectra for each are averaged over the hour of interest, and the output of the spectral wave model[2] WAVEWATCH III (WW3: Tolman et al. 2014) was interpolated to the ship location.

a. Case study: Into-waves

Figure 2 is an example of DC steaming into waves with θ_w from the MR. Over the hour, the mean ship velocity was $1.1\,\mathrm{m\,s}^{-1}$ and there was little variation. Therefore, the corrected and uncorrected spectra are similar. Within the hour the ship was turning and three members were discarded from the EM. In comparison to SM, this

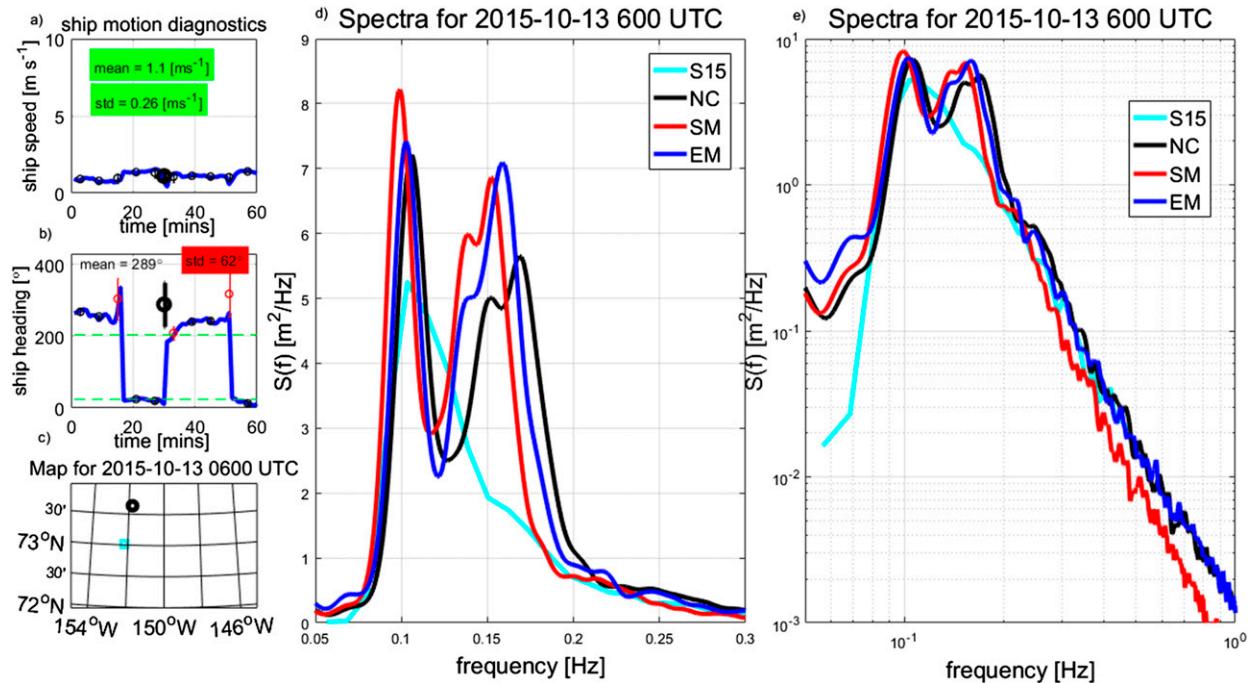[2] Details can be found in supplemental material.

FIG. 2. Case study of DC for steaming into waves. (a) Ship speed for each minute in the hour (blue line). Mean speed is shown with the large black circle with the means for each section in small black circles, and the error bars are one standard deviation. Small circles plotted in red are excluded from EM. (b) As in (a), but for ship heading. Green dashed lines show the divisions between into-waves and with-waves (green). (c) Map showing the ship (black) and the closest sensor with S15 (SWIFT buoys; cyan). (d) Spectral density for the S15 (cyan), the laser rangefinder with no correction (NC; black), SM (red), and EM (blue). (e) As in (d), but on a log scale and a longer frequency range to emphasize the high frequencies.

improved the location of f_p and the level of high-frequency energy at frequencies greater than $2.5f_p$. There was a significant secondary peak in the spectrum near 0.16 Hz not found in the buoy spectra.

b. Case study: With-waves

Figure 3 is an example of a DC in dominant with-waves conditions and θ_w from the MR. Over the hour, the mean ship speed is $3.62 \, \mathrm{m \, s^{-1}}$ with some significant variation in the speed. The heading also changed significantly, so there were times with ship steaming both with waves and into waves. Since SM used the mean over the hour, the average effective heading did not correspond to an actual heading, but it did slightly improve the position of f_p compared to no DC. EM shifted the location of f_p and the energy in the high frequencies closer to those of the nearest buoy.

c. Overall statistics

The statistics between the laser rangefinder and other sensors (plus the model) were calculated. The sensors were variable distances from the ship, so in addition to the all-encompassing dataset, a subset was examined separately that was composed of only the

nearest buoy to the ship each hour and never farther than 50 km.

Measures that emphasize the frequency of the peak of the spectrum are useful indicators for the effectiveness of DC. Two, T_p and T_4, were compared as shown:

$$T_p = 1/f_p, \tag{11}$$

$$f_p = \max_f[S(f)], \tag{12}$$

$$T_4 = \frac{\int_{f_1}^{f_2} S^4(f) \, df}{\int_{f_1}^{f_2} f S^4(f) \, df}, \tag{13}$$

where $f_1 = 0.045$ Hz and $f_2 = 0.45$ Hz. The number of samples, bias, root-mean-square error (RMSE), and Pearson's correlation coefficient R can be found in Table 1 for both the overall dataset and the nearest buoy subset.

4. Discussion

Ambiguities were resolved by attributing the energy to the lowest frequency branch solution and ignoring the
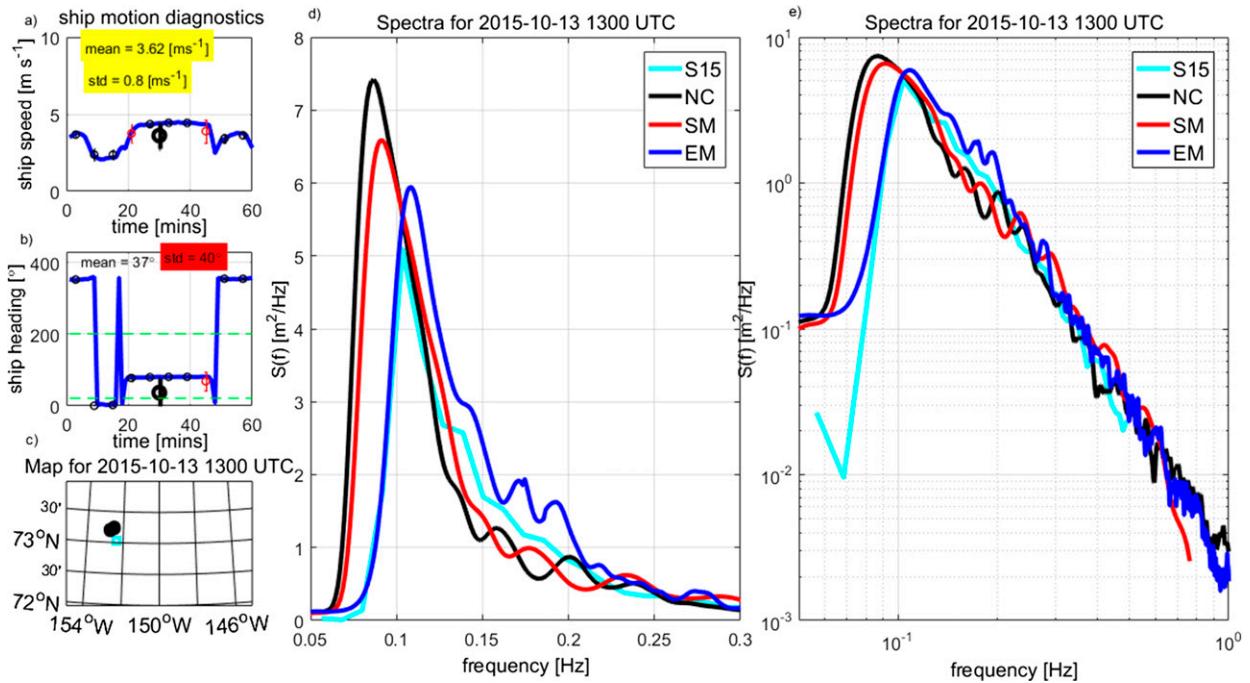
FIG. 3. Case study of DC for steaming with waves. (a) Ship speed for each minute in the hour (blue line). Mean speed is shown with the large black circle with the means for each section in small black circles, and the error bars are one standard deviation. Small circles in red are excluded from EM. (b) As in (a), but for ship heading. Green dashed lines show the divisions between into-waves and with-waves (green). (c) Map showing ship (black) and the closest sensor, S15 (cyan). (d) Spectral density for S15 (cyan), the laser rangefinder with NC (black), SM (red), and EM (blue). (e) As in (d), but on a log scale and longer frequency range to emphasize the high frequencies.

other solutions. In the case of Fig. 3, the ship speed was on average $3.6 \, \text{m s}^{-1}$ but the heading varied considerably, going both into-waves and with-waves. The ensemble method, in addition to removing short sections of high variability, coherently integrated sections with variable spectral resolutions and ranges.

Using just the lowest frequency branch in this primarily with-waves scenario gave reasonable results that

appear to properly correct for the Doppler shift. In general, using the first branch solution is expected to work well if f_p lies within this branch because wave energy beyond f_p tends to decay with an f^{-4} or f^{-5} dependency in wind-sea spectra, with even stronger decay expected in ice. As the vessel speed increases, the range of the lowest frequency branch decreases. At the R/V *Sikuliaq*'s top speed, $7.3 \, \text{m s}^{-1}$ and steaming exactly with

TABLE 1. Statistics for spectral parameters.

	Full dataset buoys + WW3					Just the nearest buoy				
		Constant		MR			Constant		MR	
T_p θ_w	NC	SM	EM	SM	EM	NC	SM	EM	SM	EM
Sample No.	443	443	443	443	443	56	56	56	56	56
Bias (s)	0.46	−0.06	−0.21	−0.17	−0.36	0.4	−0.09	−0.29	−0.3	−0.51
RMSE (s)	2.03	0.99	0.99	0.92	1	2.07	0.98	0.98	0.83	1.02
R	0.38	0.61	0.65	0.68	0.72	0.5	0.69	0.73	0.81	0.78
	Full dataset buoys + WW3					Just the nearest buoy				
		Constant		MR			Constant		MR	
T_4 θ_w	NC	SM	EM	SM	EM	NC	SM	EM	SM	EM
Sample No.	272	272	272	272	272	32	32	32	32	32
Bias (s)	−1.39	−0.73	−0.82	−0.77	−0.83	−1.39	−0.61	−0.75	−0.8	−0.86
RMSE (s)	1.73	1.17	1.15	0.98	1.04	1.75	1.09	1.04	0.97	0.99
R	0.57	0.6	0.69	0.79	0.82	0.68	0.7	0.8	0.87	0.91

the waves, the f_{cr} is just under 0.08 Hz. If this were the case, this method would not capture the energy containing region of the spectrum centered around 0.10 Hz. Situations in the field may vary, due to either the vessel velocity or the encountered wave spectrum, and the solution presented here may be inadequate. Also, the effect that ignoring other branches has on the resulting shape of the spectrum has not been determined here.

According to Table 1, the best statistics resulted from using θ_w from the marine radar and the EM Doppler correction. However, the difference between the SM and the EM was marginal. The EM avoids short time-scale variability. This could be optimized to some extent by allowing for variable size of the analysis window and/or centering windows on periods with a more stationary ship vector. This was not pursued because the guiding parameters for designing the algorithm were 1) simplicity and 2) results compatible with the other sensors. It is hypothesized that using an algorithm that optimizes the analysis window length around the stationarity of the ship vector would further improve the results.

Statistically, a more significant improvement comes from using θ_w sourced from the MR. It is perhaps obvious that a measured θ_w would be better than an assumed θ_w, but the MR offers several advantages over the alternatives: direction determined from wind or drift are not necessarily aligned with waves; buoys may not adequately represent wave directions local to the ship and have limited directional resolutions (Longuet-Higgins et al. 1963; Collins et al. 2014; Donelan et al. 2015); and good model performance is never guaranteed.

There was a secondary spectral peak in Fig. 2 not seen in the buoy spectra. We suspect this is an artifact related to ship pitch; this is discussed in the supplemental material. Keep in mind that although DC can shift the spectra by accounting for the vector velocity of the vessel, it does nothing to mitigate other errors that may arise as a result of making measurements from an underway vessel.

Neither the case of θ_w varying as a function of frequency nor the effects of directional spread were considered; these will be addressed in a future study. Currents in this area were second order to the vessel velocity, but they were a source of inaccuracy.

5. Outcome

As this study explains and demonstrates, Doppler correction can be done effectively for arbitrary cases of relative vessel heading and wave direction. Ambiguities are resolved by attributing the energy to the lowest-frequency (f_{in}) solution branch and ignoring the other branches. In addition, a practical method for handling

situations when the vessel is accelerating or changing heading is provided. Looking outward, these results could be used to Doppler-correct Eulerian wave spectra in the presence of strong currents (Steele 1997).

REFERENCES

Cifuentes-Lorenzen, A., J. B. Edson, C. J. Zappa, and L. Bariteau, 2013: A multisensor comparison of ocean wave frequency spectra from a research vessel during the Southern Ocean Gas Exchange Experiment. *J. Atmos. Oceanic Technol.*, **30**, 2907–2925, doi:10.1175/JTECH-D-12-00181.1.

Collins, C. O., III, B. Lund, R. Ramos, W. Drennan, and H. Graber, 2014: Wave measurement intercomparison and platform evaluation during the ITOP (2010) experiment. *J. Atmos. Oceanic Technol.*, **31**, 2309–2329, doi:10.1175/JTECH-D-13-00149.1.

Doble, M. J., G. De Carolis, M. H. Meylan, J.-R. Bidlot, and P. Wadhams, 2015: Relating wave attenuation to pancake ice thickness, using field measurements and model results. *Geophys. Res. Lett.*, **42**, 4473–4481, doi:10.1002/2015GL063628.

Donelan, M., A. Babanin, E. Sanina, and D. Chalikov, 2015: A comparison of methods for estimating directional spectra of surface waves. *J. Geophys. Res. Oceans*, **120**, 5040–5053, doi:10.1002/2015JC010808.

Drennan, W. M., M. A. Donelan, N. Madsen, K. B. Katsaros, E. A. Terray, and C. N. Flagg, 1994: Directional wave spectra from a Swath ship at sea. *J. Atmos. Oceanic Technol.*, **11**, 1109–1116, doi:10.1175/1520-0426(1994)011<1109:DWSFAS>2.0.CO;2.

Hanson, K. A., T. Hara, E. J. Bock, and A. B. Karachintsev, 1997: Estimation of directional surface wave spectra from a towed research catamaran. *J. Atmos. Oceanic Technol.*, **14**, 1467–1482, doi:10.1175/1520-0426(1997)014<1467:EODSWS>2.0.CO;2.

Kats, A. V., and I. S. Spevak, 1980: Reconstruction of the sea-wave spectra from measurements of moving sensors. *Izv., Acad. Sci., USSR, Atmos. Oceanic Phys.*, **16**, 194–200.

Kinsman, B., 1965: *Wind Waves, Their Generation and Propagation on the Ocean Surface.* Prentice-Hall, 676 pp.

Kohout, A. L., B. Penrose, S. Penrose, and M. J. Williams, 2015: A device for measuring wave-induced motion of ice floes in the Antarctic marginal ice zone. *Ann. Glaciol.*, **56**, 415–424, doi:10.3189/2015AoG69A600.

Lamb, H., 1932: *Hydrodynamics*. Cambridge University Press, 738 pp.

Longuet-Higgins, M. S., D. E. Cartwright, and N. D. Smith, 1963: Observations of the directional spectrum of sea waves using the motions of a floating buoy. *Ocean Wave Spectra: Proceedings of a Conference*, Prentice-Hall, 111–136.

Lund, B., H. C. Graber, K. Hessner, and N. J. Williams, 2015: On shipboard marine X-band radar near-surface current "calibration." *J. Atmos. Oceanic Technol.*, **32**, 1928–1944, doi:10.1175/JTECH-D-14-00175.1.

——, C. O. Collins III, H. Tamura, and H. C. Graber, 2016: Multidirectional wave spectra from marine X-band radar. *Ocean Dyn.*, **66**, 973–988, doi:10.1007/s10236-016-0961-z.

Steele, K. E., 1997: Ocean current kinematic effects on pitch–roll buoy observations of mean wave direction and nondirectional spectra. *J. Atmos. Oceanic Technol.*, **14**, 278–291, doi:10.1175/1520-0426(1997)014<0278:OCKEOP>2.0.CO;2.

Thomson, J., 2012: Wave breaking dissipation observed with "SWIFT" drifters. *J. Atmos. Oceanic Technol.*, **29**, 1866–1882, doi:10.1175/JTECH-D-12-00018.1.

——, and Coauthors, 2013: Science plan: Sea state and boundary layer physics of the emerging Arctic Ocean. Applied Physical Laboratory Tech. Rep. APL-UW TR1306, University of Washington, 58 pp.

Tolman, H. L., and Coauthors, 2014: User manual and system documentation of WAVEWATCH III version 4.18. NOAA/NWS/NCEP/MMAB Tech. Note 316, 311 pp.

Wadhams, P., V. A. Squire, D. J. Goodman, A. M. Cowan, and S. C. Moore, 1988: The attenuation rates of ocean waves in the marginal ice zone. *J. Geophys. Res.*, **93**, 6799–6818, doi:10.1029/JC093iC06p06799.